



**HAL**  
open science

## Stable and inert manganese complexes for magnetic resonance imaging

Daouda Ndiaye, Éva Tóth

► **To cite this version:**

Daouda Ndiaye, Éva Tóth. Stable and inert manganese complexes for magnetic resonance imaging. Comptes Rendus. Chimie, 2024, 27 (S2), pp.161 - 177. 10.5802/crchim.284 . hal-04780758

**HAL Id: hal-04780758**

**<https://hal.science/hal-04780758v1>**

Submitted on 13 Nov 2024

**HAL** is a multi-disciplinary open access archive for the deposit and dissemination of scientific research documents, whether they are published or not. The documents may come from teaching and research institutions in France or abroad, or from public or private research centers.

L'archive ouverte pluridisciplinaire **HAL**, est destinée au dépôt et à la diffusion de documents scientifiques de niveau recherche, publiés ou non, émanant des établissements d'enseignement et de recherche français ou étrangers, des laboratoires publics ou privés.



Distributed under a Creative Commons Attribution 4.0 International License



ACADÉMIE  
DES SCIENCES  
INSTITUT DE FRANCE

# *Comptes Rendus*

---

## *Chimie*

Daouda Ndiaye and Éva Tóth

**Stable and inert manganese complexes for magnetic resonance imaging**

Volume 27, Special Issue S2 (2024), p. 161-177


Online since: 28 February 2024

Issue date: 11 July 2024

**Part of Special Issue:** Women Chemists in France in 2024

**Guest editor:** Janine Cossy (ESPCI Paris – PSL, CNRS, 75005 Paris, France)

<https://doi.org/10.5802/crchim.284>

 This article is licensed under the  
CREATIVE COMMONS ATTRIBUTION 4.0 INTERNATIONAL LICENSE.  
<http://creativecommons.org/licenses/by/4.0/>



*The Comptes Rendus. Chimie are a member of the  
Mersenne Center for open scientific publishing*  
[www.centre-mersenne.org](http://www.centre-mersenne.org) — e-ISSN : 1878-1543



Research article

Women Chemists in France in 2024

# Stable and inert manganese complexes for magnetic resonance imaging

Daouda Ndiaye<sup>a</sup> and Éva Tóth<sup>\*,\*,a</sup>

<sup>a</sup> Centre de Biophysique Moléculaire, CNRS UPR4301, Université d'Orléans,  
Rue Charles Sadron, 45071 Orléans, France

Current address: Laboratoire Chimie et Biologie des Métaux, CEA-Grenoble, France  
(D. Ndiaye)

E-mail: [eva.jakabtoth@cnrs-orleans.fr](mailto:eva.jakabtoth@cnrs-orleans.fr) (É. Tóth)

**Abstract.** Paramagnetic  $Mn^{2+}$  complexes are intensively investigated as alternatives to replace the currently used, Gd-based clinical contrast agents in Magnetic Resonance Imaging (MRI). Manganese is an essential metal which alleviates its potential toxicity and the environmental concerns related to the use of  $Gd^{3+}$ . Thanks to its five unpaired electrons and slow electron spin relaxation,  $Mn^{2+}$  is a very efficient relaxation agent. Given the high doses required for *in vivo* MRI,  $Mn^{2+}$  needs to be chelated in thermodynamically stable and kinetically inert complexes, despite its natural presence in the body. We survey here the latest developments in the chemistry and the preliminary *in vivo* MRI evaluation of  $Mn^{2+}$  complexes. We specifically focus on the molecular ligand design, including linear, macrocyclic and bicyclic (bispidine) chelators that allowed for substantially enhanced kinetic inertness of the complexes, as well as for ligand selectivity for  $Mn^{2+}$  versus the main biological competitor  $Zn^{2+}$ . In addition to the +2 form of manganese,  $Mn^{3+}$  is also paramagnetic in the high-spin state, with promising relaxation properties among porphyrin complexes. Finally, examples will be presented to demonstrate the first steps towards the development of redox sensors based on the  $Mn^{2+}/Mn^{3+}$  switch, detectable in  $^1H$  or in  $^{19}F$  MRI.

**Keywords.** Manganese, MRI contrast agent, Relaxation agent, Bispidine.

Manuscript received 28 November 2023, revised and accepted 15 January 2024.

## 1. Introduction

Starting with the discovery of X-ray at the end of the 19th century and its immediate application to visualize the inside of the body [1], imaging technologies have revolutionized the way medical doctors work. The imaging field witnessed a spectacular progress from the 1970s, with the introduction of computerized image construction procedures as well as novel technologies based on various physical phenomena, including ultrasound, magnetic resonance

or radioactive emission. Imaging has also become a major investigation tool in biological research to understand function and distribution of biomolecules *in vivo* or *in cellulo*. Finally, the pharmaceutical industry is also increasingly integrating imaging into the drug development process, to follow drug biodistribution, metabolic fate or therapeutic effect.

Introduced in the early 1980s, Magnetic Resonance Imaging (MRI) has become a widespread and powerful tool for establishing clinical diagnosis and monitoring therapy. The use of paramagnetic metal complexes as contrast-enhancing agents has greatly contributed to this success [2]. MRI is based on

\*Corresponding author

the nuclear relaxation properties of mostly water protons. Paramagnetic (or superparamagnetic) materials can substantially reduce the relaxation rates of surrounding nuclei, thereby improving image contrast between different tissues [3].

Today, clinically approved MRI contrast agents are complexes of the rare earth metal ion gadolinium ( $\text{Gd}^{3+}$ ). With its seven unpaired electrons ( $S = 7/2$ ) and exceptionally slow electron spin relaxation due to a symmetric electron configuration,  $\text{Gd}^{3+}$  is the most paramagnetic metal ion in the periodic table and a very efficient relaxation agent.  $\text{Gd}^{3+}$  complexes were considered for a long time as safe drugs which are fully eliminated from the body shortly after their injection. However, since 2006, several  $\text{Gd}^{3+}$ -related toxicity cases were reported, mostly in kidney-impaired patients presenting slow renal excretion [4]. In this novel, occasionally fatal disease called nephrogenic systemic fibrosis, Gd deposition was detected in the body, originating from the dissociation of the injected agent releasing free, non-complexed  $\text{Gd}^{3+}$ . This could be directly related to the low kinetic inertness, thus low resistance of the chelates to dissociation. The drug safety agencies in the USA and Europe rapidly responded by the withdrawal of several, less inert chelates and by restricting the use of any  $\text{Gd}^{3+}$ -based agent in kidney-impaired patients. Long-term accumulation of very small, but detectable amounts of  $\text{Gd}^{3+}$  has been also observed in various organs of patients, without toxic effects [5]. Lately, the presence of Gd in river and coastal waters due to contrast agent applications is arising as an important environmental pollution issue [6,7]. Altogether, these problems have promoted intensive research in the community of coordination chemists to identify safer alternatives to  $\text{Gd}^{3+}$  complexes.

Among potential metal ions,  $\text{Mn}^{2+}$  is the most obvious candidate to replace  $\text{Gd}^{3+}$  in MRI contrast agent applications [8,9]. In its high-spin state,  $\text{Mn}^{2+}$  has five unpaired electrons ( $S = 5/2$ ) and slow electron spin relaxation, which are the most critical requirements for a significant relaxation effect. The first relaxation agent used in MRI by Lauterbur was  $\text{MnCl}_2$  [10], and  $\text{Mn}^{2+}$  continues to be applied in specific animal experiments to track excitable cells like neurons and cardiac cells where it enters as a  $\text{Ca}^{2+}$  surrogate (Manganese-Enhanced MRI = MEMRI) [11].

Manganese is an essential metal, having multiple biological roles. Despite the natural presence of manganese in the body, injecting free  $\text{Mn}^{2+}$  at the typically high MRI contrast agent doses (0.05–0.30 mmol per kg body weight) could be problematic, potentially causing neurotoxicity and Parkinson-like symptoms [12]. Therefore,  $\text{Mn}^{2+}$  needs to be chelated in stable and inert complexes for *in vivo* applications.

In this context, a great number of novel ligands have been proposed for  $\text{Mn}^{2+}$  chelation during the last decade [8,13]. Stable and inert complexation of  $\text{Mn}^{2+}$  is, however, a coordination chemistry challenge. Indeed, in the high spin  $d^5$  electron configuration,  $\text{Mn}^{2+}$  has no ligand-field stabilization energy, thus its complexes are less stable than those formed with other divalent transition metal analogues, including the most relevant biological competitor  $\text{Zn}^{2+}$ . The thermodynamic stability of the metal chelates is expressed by the stability constant,  $\log K_{\text{ML}}$  ( $K_{\text{ML}} = [\text{ML}]/[\text{M}][\text{L}]$ , where the values in brackets correspond to equilibrium concentrations of the complex ML, the metal M and the fully deprotonated ligand L, respectively). Conditional stabilities are often compared for different complexes in order to get rid of the difference in ligand protonation constants. For potential  $\text{Mn}^{2+}$ -based contrast agents, conditional stability is most commonly expressed with the  $\text{pMn} = -\log[\text{Mn}]$  value, where  $[\text{Mn}]$  is the equilibrium concentration of free  $\text{Mn}^{2+}$ , calculated for  $10^{-5}$  M total concentrations of the metal and the ligand each, at pH 7.4 [14]. In addition to the thermodynamic stability, the kinetic inertness, i.e. resistance of the chelate to dissociation, which would lead to the release of free metal ion in biological media, is another important requirement for *in vivo* use. Dissociation of metal complexes typically occurs by acid- and metal-mediated processes. Concerning the metal-catalysis, endogenous metal ions, such as  $\text{Cu}^{2+}$  or  $\text{Zn}^{2+}$  are the most important to promote transmetallation, thus  $\text{Mn}^{2+}$  release [15]. Kinetic inertness is often regarded as even more relevant than high thermodynamic stability, because once the complex is injected into the body, it is not in thermodynamic equilibrium; yet it should stay intact all along its way through the body until full excretion.  $\text{Mn}^{2+}$  complexes are typically labile, and until very recently, it seemed extremely challenging to attain substantial increase in their kinetic inertness.

For good MRI efficiency,  $\text{Mn}^{2+}$  complexes need to contain at least one water molecule in their inner coordination sphere which makes high thermodynamic stability and kinetic inertness even more difficult to achieve. The MRI efficiency of a contrast agent is given by its relaxivity ( $r_1$ ), which is defined as the paramagnetic enhancement of the longitudinal water proton relaxation rate induced by a unity (millimolar) concentration of the probe (the metal ion) [3]. The relaxation effect of the paramagnetic metal complex on the surrounding water protons is governed by two major contributions, called outer and inner sphere relaxivity, both linearly dependent on  $S(S+1)$ . This implies that relaxivities will be lower for  $\text{Mn}^{2+}$  ( $S = 5/2$ ) than for  $\text{Gd}^{3+}$  ( $S = 7/2$ ) complexes provided the other determining parameters are similar [16], thus higher doses might be required for  $\text{Mn}^{2+}$ -based MRI agents to achieve a similar contrast enhancement effect.

Outer sphere relaxivity arises from dipole–dipole interactions between the electron spin of the metal and the nuclear spin of the water protons diffusing around the complex. The inner-sphere term, which is more interesting since it can be optimized by rational molecular design, is related to water (or proton) exchange between the inner sphere of the metal ion and bulk water. As dipolar interactions are strongly dependent on the distance between the electron and nuclear spins, inner sphere protons experience a much stronger paramagnetic relaxation effect, and this is then transferred to the surrounding water by chemical exchange of the inner sphere water. Inner sphere relaxivity is thus dependent on different structural and dynamic parameters of the complex, such as the number of water molecules directly coordinated to the metal ion (hydration number,  $q$ ), the rate of exchange of these water molecules with bulk water ( $k_{\text{ex}}$ ), the rotational motion of the complex characterized by the rotational correlation time ( $\tau_R$ ), and the relaxation times of the electron spin of the metal ( $T_{1e}$  and  $T_{2e}$ ). Inner sphere relaxivity is linearly proportional to the hydration number, however, given the relatively low stability of  $\text{Mn}^{2+}$  complexes, it seems difficult to increase relaxivity by designing bishydrated chelates.

One  $\text{Mn}^{2+}$  complex was previously approved for clinical contrast agent use (Teslascan<sup>®</sup>), but later withdrawn. This non-hydrated MnDPDP chelate (DPDP = N,N'-dipyridoxylethylenediamine-N,N'-

diacetate-5,5'-bis(phosphate); Scheme 1) is not stable *in vivo*, but releases free  $\text{Mn}^{2+}$  which is mostly responsible for its relaxation effect. Although no toxicity problems were associated to the use of MnD-PDP, it is obvious that today no  $\text{Mn}^{2+}$  complex with such limited stability could be accepted for human applications.

Beside the 2+ oxidation state, manganese can also exist as a  $\text{Mn}^{3+}$  cation in aqueous solution, including under biological conditions. High spin  $\text{Mn}^{3+}$  is also paramagnetic. Although  $\text{Mn}^{3+}$  has lower electron spin ( $S = 4/2$ ) and typically faster electron spin relaxation than  $\text{Mn}^{2+}$ , several examples, in particular in the family of  $\text{Mn}^{3+}$  porphyrin complexes, evidence that this higher oxidation state can also have interesting relaxation properties with potential applications in MRI [17].

In addition, the transformation between the  $\text{Mn}^{3+}$  and  $\text{Mn}^{2+}$  forms mediated by biological redox active species can be exploited for the design of redox responsive MRI probes. As the  $\text{Mn}^{3+}$  and  $\text{Mn}^{2+}$  states are characterized by different relaxation properties, a redox change will be detectable on the Magnetic Resonance images, and this can report on the redox state of the biological environment [18].

We should also mention that Mn has a positron-emitting radionuclide,  $^{52}\text{Mn}$ , with interesting decay features for application in Positron Emission Tomography (PET) ( $t_{1/2} = 5.6$  d,  $\beta^+$ -decay intensity: 29.6%, max.  $\beta^+$ -energy: 575 keV). The relatively long half-life makes  $^{52}\text{Mn}$  suitable for the imaging of the slow biodistribution of macromolecules (such as monoclonal antibodies), over periods of days. For PET applications, highly stable and inert Mn chelation is very important to prevent off-target signals originating from released free  $^{52}\text{Mn}$ .

The increasing interest in  $^{52}\text{Mn}$  is also related to the important advances in bimodal PET/MRI.  $\text{Mn}^{2+}$  is the only example where a *unique* metal ion offers detection capability in both MRI and PET, which obviously alleviates the chemical design of bimodal PET/MRI agents [19]. Instead of conjugating individual PET and MRI probes, an appropriate isotopic  $^{52/\text{nat}}\text{Mn}$  mixture provides the bimodal PET/MR tracer with ease, ensures that PET and MR reporter complexes are present in a concentration adapted for each imaging modality (PET is  $>10^6$  times more sensitive than MRI) and have strictly identical *in vivo* biodistribution.

In overall, for any bioimaging application,  $\text{Mn}^{2+}$  needs to be chelated in complexes of high thermodynamic stability and kinetic inertness. When MRI applications are concerned, such high stability and inertness of the complex need to be maintained while preserving one inner sphere water molecule to ensure relaxation efficiency. Another feature to consider is the rich redox chemistry of Mn, which implies that the ligand should stabilize the required redox state under biological conditions. To meet all these requirements together, novel ligands have to be designed.

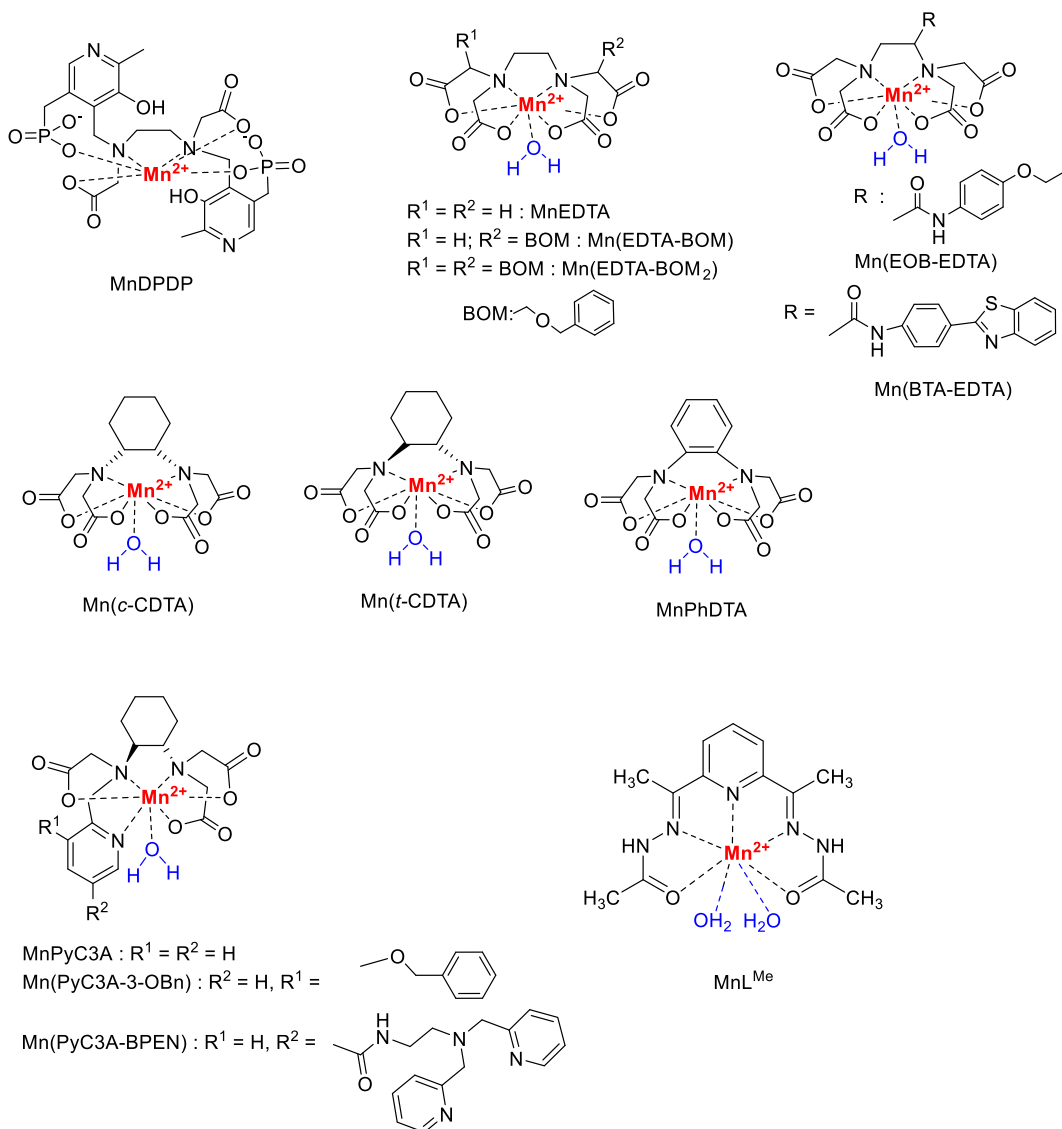
Here, we give an overview of the recent advances in the development of Mn-based potential MR imaging agents. In parallel to the on-going progress in the chemistry of imaging agents, the first steps have also been made towards clinical translation, as two small molecular weight  $\text{Mn}^{2+}$  chelates passed to Phase 1 human trials as potential extracellular, “general-purpose” MRI probes to replace the current  $\text{Gd}^{3+}$ -based agents [20,21]. Our objective is not to be exhaustive in this review. We will mainly focus on the chemical design of the ligand in order to tackle the most challenging questions: how to improve the kinetic inertness for the  $\text{Mn}^{2+}$  complexes and how to achieve selectivity for  $\text{Mn}^{2+}$  over the main biological competitor  $\text{Zn}^{2+}$ . While we will select examples from different ligand families including also the design of smart imaging agents, derived from the best chelators, we will survey more closely the latest results obtained with bispidine-type complexes, which brought spectacular progress in these respects. Finally, concerning  $\text{Mn}^{3+}$  chelates, there is much less data available in the literature, but some recent examples indicate that novel opportunities might be opened in this field.

## 2. Linear chelators for $\text{Mn}^{2+}$ complexation

$\text{Mn}^{2+}$  complexes of ethylenediamine-tetraacetate (EDTA) and its derivatives have been known for more than 50 years. These chelates are typically seven-coordinated with one inner sphere water molecule, which made them also interesting early on for paramagnetic relaxation studies [22]. In the context of MRI contrast agent development, derivatization of MnEDTA with hydrophobic moieties such as an ethoxybenzyl (EOB), a benzothiazole-aniline (BTA) or a benzyloxymethyl (BOM) has

been more recently reported to target the liver (Mn(EOB-EDTA), Mn(BTA-EDTA)) [23,24] or to induce non-covalent binding to human serum albumin (Mn(EDTA-BOM)) [25] for angiographic imaging (Scheme 1). These modifications influence the biological fate of the complexes, but have limited impact on their thermodynamic stability or kinetic inertness, and in particular, this latter remains relatively low. The relaxivity is slightly increased for Mn(EDTA-BOM) or Mn(EDTA-BOM<sub>2</sub>) complexes (3.60 and 4.30  $\text{mM}^{-1}\cdot\text{s}^{-1}$ , 20 MHz, 25 °C) [25] versus MnEDTA (3.00  $\text{mM}^{-1}\cdot\text{s}^{-1}$ ) [25], in accordance with the increased molecular size.

The most important developments in this family concern the rigidification of the ligand skeleton in the objective of improving kinetic inertness. Several design elements have been tested in this direction. First of all, the ethylene backbone was replaced with considerably less flexible moieties such as a cyclohexane, a benzene or a pyridine ring, and this led to improved resistance to complex dissociation. The effect of rigidity was first demonstrated by comparing the kinetic inertness of MnEDTA and Mn(*t*-CDTA) (*t*-CDTA = *trans*-1,2-diaminocyclohexane-*N,N,N',N'*-tetraacetate; Scheme 1) in  $\text{Cu}^{2+}$  exchange reactions [26]. These evidenced a two orders of magnitude slower proton-assisted dissociation for Mn(*t*-CDTA), resulting in a dissociation half-life of  $t_{1/2} = 12$  h estimated for physiological conditions, versus 0.076 h for MnEDTA (pH 7.4 and  $10^{-5}$  M  $\text{Cu}^{2+}$  concentration). The two stereoisomer forms of the cyclohexane-based CDTA ligand, the *trans t*-CDTA and the *cis c*-CDTA provide a different coordination cage for metal complexation; it is considerably larger for *t*-CDTA with a maximum distance of 4 Å between the two nitrogen atoms, as compared to 3.1 Å for *c*-CDTA [27]. Yet, DFT calculations indicate only minor differences in the metal coordination environments in the solution structures, with bond distances differing in less than 0.035 Å. The DFT results suggest remarkably higher stability for the *trans* than for the *cis* analogue, with an energy difference of 35.4  $\text{kJ}\cdot\text{mol}^{-1}$ . This was linked to the more strained geometry of the ligand in the *cis*- than in the *trans*-stereoisomer in accommodating the relatively large  $\text{Mn}^{2+}$  ion [28]. Experimental data confirm these findings. Although the thermodynamic stability constants for Mn(*c*-CDTA) and Mn(*t*-CDTA) are similar ( $\log K_{\text{MnL}}$  values are 14.19 and 14.32, respectively), the



**Scheme 1.** Mn<sup>2+</sup> complexes formed with linear ligands.

conditional stability as expressed by the pMn value is higher for Mn(*t*-CDTA) (8.68 versus 7.82;  $c_L = c_{Mn} = 10^{-5}$  M, pH 7.4). The most striking difference is in the kinetic inertness of the complexes, the *trans*-isomer being 250 times more inert than the *cis*-analogue, as it was assessed in Cu<sup>2+</sup> transmetalation reactions [28]. The *t*-CDTA was then used for the development of a bifunctional chelator, and the Mn<sup>2+</sup> complex was evaluated with respect to its MRI properties [29].

The kinetic inertness is further improved with the PhDTA ligand, where an aromatic benzene ring rigidifies the molecular skeleton (PhDTA = *o*-phenylenediamine-*N,N,N',N'*-tetraacetate; Scheme 1). The dissociation half-life of MnPhDTA is estimated to be  $t_{1/2} = 19$  h at pH 7.4 [30]. On the other hand, the conditional stability constant (pMn = 8.16) and the relaxivity (3.72 mM<sup>-1</sup>·s<sup>-1</sup>; 20 MHz, 25 °C) remain similar to those of Mn(*t*-CDTA). Other ligands containing a pyridine in their backbone were

also investigated, however, these ligands did not lead to improved inertness of the  $\text{Mn}^{2+}$  complexes [31].

Amphiphilic anionic *t*-CDTA derivatives have been recently reported for specific uptake by hepatocytes through one or two bi-directional transmembrane Organic Anion Transporting Polypeptide (OATP) transporters. The complexes have been characterized through relaxivity measurements, *in vivo* liver imaging in mice, and quantitation of *in vitro* cell uptake through ectopically expressed human OATP1 transporters [32].

The group of Caravan developed the N-picolyl-N,N',N'-trans-1,2-cyclohexylenediaminetriacetate (PyC3A; Scheme 1) ligand by further rigidifying *t*-CDTA by the substitution of one carboxylate with a pyridine. MnPyC3A was proposed in 2015 as an extracellular contrast agent alternative to  $\text{Gd}^{3+}$ -based contrast agents [33], and it reached Phase 1 human studies in 2022 [20]. MnPyC3A is endowed with good thermodynamic and conditional stability ( $\log K_{\text{MnL}} = 14.14$  and  $\text{pMn} = 8.17$ ), and its kinetic inertness exceeds that of the clinical contrast agent GdDTPA; in the presence of 25-fold excess of  $\text{Zn}^{2+}$ , pH 6, 37 °C, the dissociation is 20-times faster for GdDTPA than for MnPyC3A. The relaxivity of MnPyC3A is  $3.3 \text{ mM}^{-1}\cdot\text{s}^{-1}$  (20 MHz, 25 °C), in coherence with its molecular size and monohydrated nature, and it is slightly increased in serum due to moderate interaction with serum proteins.

Thanks to its slightly lipophilic structure, MnPyC3A undergoes combined hepatobiliary and renal excretion, and no *in vivo* degradation was detected for the complex. MR Imaging evaluation of this potential contrast agent has been realized in various animal models with side-by-side comparison to clinical agents. In a nonhuman primate model, MnPyC3A provided signal enhancement in arteries versus muscle which was comparable to GdDTPA in a standard dynamic MR angiography protocol [34]. Pharmacokinetics was also found comparable to that of clinically used extracellular Gd-based agents [34]. In rat models of breast cancer and metastatic liver disease, it was found to be equally efficient to delineate tumors as the clinical  $\text{Gd}^{3+}$  probes [35]. MnPyC3A was recently tested in pigs for tissue characterization of acute myocardial infarction, and it appeared to be equally effective as gadolinium-based agents for the assessment of myocardial infarction location and size [36].

Several liver-specific probes have been also derived from MnPyC3A. In a family of nine complexes, a lead compound substituted with a benzyloxy-moiety on the pyridine was retained based on its high relaxivity, rapid blood clearance and avid hepatocellular uptake, the two latter properties directly correlated with the  $\log P$  values [37]. Injection of this lead Mn(PyC3A-3-OBn) complex (Scheme 1) into a mouse model with colorectal liver metastasis resulted in excellent tumor visualization as hypointense spots.

MnPyC3A was conjugated to bis-pyridyl-ethylamine (BPEN), the well-known  $\text{Zn}^{2+}$ -binding moiety, to derive a responsive agent for the *in vivo* detection of  $\text{Zn}^{2+}$  released in different mouse tissues, in particular to image  $\beta$ -cell function in the pancreas and glucose-stimulated zinc secretion in the prostate [38]. Mn(PyC3A-BPEN) (Scheme 1), like previously reported Gd-based zinc-responsive agents based on BPEN, shows only a modest  $r_1$  increase in the presence of  $\text{Zn}^{2+}$  alone, but when Human Serum Albumin (HSA) is also present, a ternary Mn(PyC3A-BPEN)-Zn-HSA complex forms with significantly enhanced relaxivity, allowing for  $\text{Zn}^{2+}$  detection. Interestingly, the presence of the BPEN unit was found to improve the kinetic inertness of the complex toward transmetalation by  $\text{Zn}^{2+}$  and transchelation by HSA. Biodistribution and excretory characterization studies indicated that Mn(PyC3A-BPEN) is eliminated from mice without dissociation, by combined renal and hepatobiliary pathways.

Stasiuk and collaborators reported a pentadentate Schiff-base type  $\text{Mn}^{2+}$  complex,  $\text{MnL}^{\text{Me}}$  which was obtained in a single-pot template reaction [39] (Scheme 1). In solution, this chelate has two inner sphere water molecules, and correspondingly elevated proton relaxivity which further increases in the presence of serum albumin ( $r_1 = 5.7 \text{ mM}^{-1}\cdot\text{s}^{-1}$  and  $21.1 \text{ mM}^{-1}\cdot\text{s}^{-1}$ , respectively, 298 K, 20 MHz). The inertness of this complex might be insufficient for further development. In the presence of 25-fold excess of  $\text{Zn}^{2+}$  at pH 6.4,  $\text{MnL}^{\text{Me}}$  was found to fully dissociate in  $\sim 10$  min. After injection of  $\text{MnL}^{\text{Me}}$  in a clinical dose ( $0.1 \text{ mmol}\cdot\text{kg}^{-1}$ ) in a healthy mouse, urine samples were collected and analyzed by LC-MS, showing that at 40 min post injection, 24% of the applied  $\text{MnL}^{\text{Me}}$  was excreted into the bladder in an intact form.



### 3. Macrocyclic chelators for Mn<sup>2+</sup> complexation

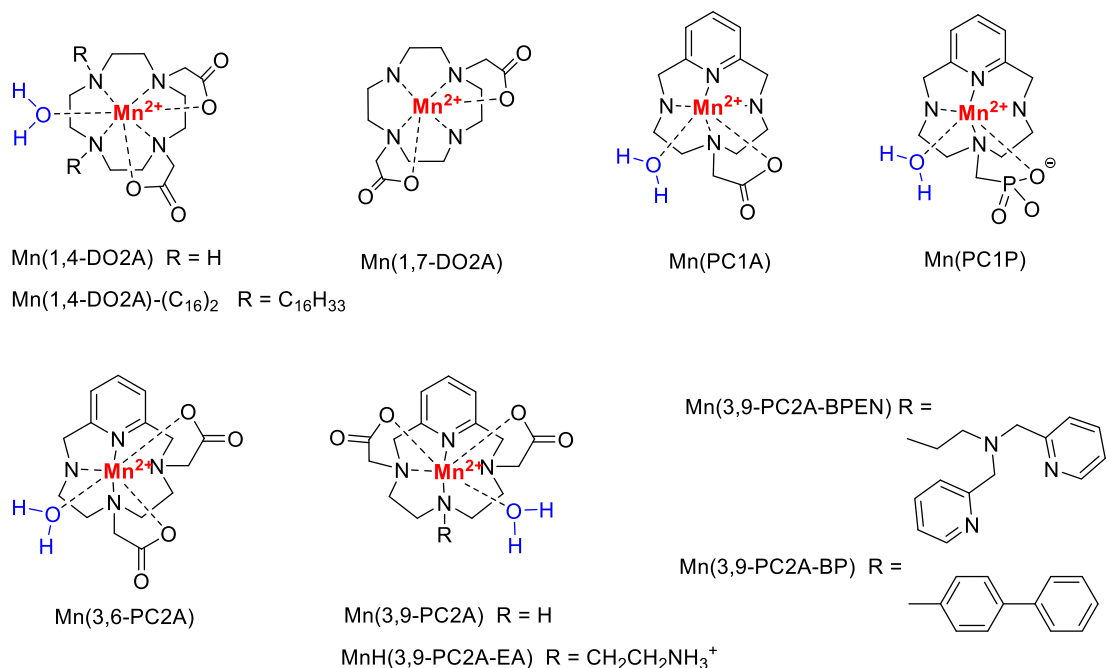
A great number of macrocycles of different sizes and bearing various coordinating functions have been investigated for Mn<sup>2+</sup> complexation in the last two decades. The most important studies involve 9-, 12- and 15-membered azamacrocycles and aza- or azoxa crown ethers, many of these have been recently reviewed [13]. We will only focus on 12-membered rings, based either on the cyclen or on the pyridine-containing pyclen macrocycle.

MnDOTA (DOTA = 1,4,7,10-tetraazacyclododecane-1,4,7,10-tetraacetate) is known for a long time to be very stable and highly inert [15,40], however, with eight coordinating functions from the ligand, there is no space for inner sphere water in this complex, which limits its relaxation efficacy to an outer sphere effect. One has to remove at least two carboxylates from DOTA to allow for inner sphere water coordination in the Mn<sup>2+</sup> complexes. Interestingly, for MnDO2A chelates, the hydration state depends on the position of the two carboxylate functions. A combined <sup>17</sup>O NMR, NMRD (Nuclear Magnetic Relaxation Dispersion) and DFT study indicated a hydration equilibrium between nonhydrated ( $q = 0$ ) and monohydrated ( $q = 1$ ) species in solution, with clear prevalence of the monohydrated form for Mn(1,4-DO2A) (average  $q$  is 0.9), while Mn(1,7-DO2A) was essentially non-hydrated (1,4-DO2A = 1,4,7,10-tetraazacyclododecane-1,4-diacetate; 1,7-DO2A = 1,4,7,10-tetraazacyclododecane-1,7-diacetate; Scheme 2) [41]. In accordance with this, proton relaxivities amount to 2.1 mM<sup>-1</sup>·s<sup>-1</sup> for Mn(1,4-DO2A) and to 1.5 mM<sup>-1</sup>·s<sup>-1</sup> for Mn(1,7-DO2A) (25 °C, 30 MHz). It is surprising that despite this difference in the coordination mode, the thermodynamic stabilities and the kinetic inertness of the two isomers are comparable [42]. A detailed transmetalation study of the complexes with Zn<sup>2+</sup> or Cu<sup>2+</sup> ions revealed that the dissociation proceeds primarily by acid catalysis, and metal-assisted pathways are negligible. The complexes are about 20 times more labile than MnDOTA, with dissociation half-lives of 48.3 h (Mn(1,4-DO2A)) and 56.8 h (Mn(1,7-DO2A)) estimated for pH 7.4, to be compared to 1061 h for MnDOTA. 1,4-DO2A was further functionalized with long aliphatic C12 and C16 chains on the secondary amines to promote micellization in solution [43].

For the corresponding Mn<sup>2+</sup> chelates, this leads to important decrease in the rotational motion, with a concomitant enhancement of the proton relaxivity, up to seven-fold at 30 MHz, where rotation is an important factor for relaxivity [ $r_1 = 15.3 \text{ mM}^{-1}\cdot\text{s}^{-1}$  for the Mn(1,4-DO2A)-(C16)<sub>2</sub> derivative with two C16 chains, 298 K (Scheme 2)].

The incorporation of a pyridine into the 12-membered cyclen macrocycle also rigidifies the molecules, as in the case the linear chelators. Monofunctionalization of this pyclen cycle with one acetate (PC1A = 6-carboxymethyl-3,6,9,15-tetraazabicyclo[9.3.1] pentadeca-1(15),11,13-triene) or one methylenephosphonate group (PC1P = 6-dihydroxyphosphorylmethyl-3,6,9,15-tetraazabicyclo[9.3.1] pentadeca-1(15),11,13-triene) results in Mn<sup>2+</sup> complexes which are six-coordinate with one inner sphere water (Scheme 2), but they do not have sufficient thermodynamic and redox stability, nor kinetic inertness [44]. Two acetate functions were introduced on the pyclen either at the 3,6 or at the 3,9 positions (3,6-PC2A and 3,9-PC2A, respectively, Scheme 2), and the corresponding Mn<sup>2+</sup> complexes were compared in a detailed physical-chemical study [45]. In contrast to the DO2A analogues, there is no difference in the hydration state of the Mn(3,6-PC2A) and Mn(3,9-PC2A) chelates, which are both monohydrated, as evidenced by <sup>17</sup>O chemical shifts and relaxation rates. The relaxivities are also similar, and typical of small monohydrated chelates (2.72 and 2.91 mM<sup>-1</sup>·s<sup>-1</sup>, for Mn(3,6-PC2A) and Mn(3,9-PC2A), respectively, 298 K, 0.49 T). The regioisomer Mn(3,9-PC2A) with the two acetate groups in *trans* position is endowed with a slightly higher thermodynamic stability constant than Mn(3,6-PC2A) ( $\log K_{\text{MnL}} = 17.09$  versus 15.53, respectively) and conditional stability ( $\text{pM} = 8.64$  versus 8.03;  $c_{\text{L}} = c_{\text{Mn}} = 10^{-5} \text{ M}$ , pH 7.4), while kinetic inertness is better for Mn(3,6-PC2A), as shown by the longer dissociation half-life calculated ( $t_{1/2} = 63.2 \text{ h}$  versus 21.0 h for Mn(3,6-PC2A) and Mn(3,9-PC2A), respectively; pH 7.4). Interestingly, DFT calculations showed important differences in some nitrogen-Mn distances between the two isomers, indicating more steric strain for Mn(3,6-PC2A), which might be the reason for its lower stability. In overall, both chelates satisfy the requirements of good stability and inertness.

The symmetrical 3,9-PC2A has been chosen for the design of various molecular imaging



**Scheme 2.** Mn<sup>2+</sup> complexes formed with macrocyclic ligands.

agents. The pH-responsive probe Mn(3,9-PC2A-EA) (Scheme 2) [46] undergoes protonation on the ethyleneamine side-chain with  $\log K_a$  of 6.88 which can thus coordinate/decoordinate to/from the metal ion as a function of its protonation state. As a consequence, the hydration number, thus the relaxivity of Mn(3,9-PC2A-EA) increases from  $q = 0$  and  $r_1 = 2.04 \text{ mM}^{-1} \cdot \text{s}^{-1}$ , respectively, at pH 8.4 to  $q = 1$  and  $r_1 = 3.54 \text{ mM}^{-1} \cdot \text{s}^{-1}$  at pH 6.0 (0.49 T, 25 °C). By attaching the BPEN Zn<sup>2+</sup> sensitive unit to 3,9-PC2A, the Zn<sup>2+</sup>-responsive probe Mn(PC2A-BPEN) was prepared (Scheme 2) [47]. This probe functions according to a similar mechanism described above for Mn(PyC3A-BPEN) by forming a ternary complex with Zn<sup>2+</sup> and HSA, accompanied by a relaxivity increase. Mn(PC2A-BPEN) could be used to visualize glucose-stimulated Zn<sup>2+</sup> secretion in the prostate of a healthy mouse.

The same 3,9-PC2A unit was also derivatized with a biphenyl moiety which induces HSA-binding (Scheme 2) [48]. This leads to a prolonged residential time of Mn(3,9-PC2A)-BP in the blood which makes it interesting for angiographic imaging. Indeed, it could be used to highlight microvasculature of the mouse brain.

#### 4. Bispidine chelators

All data on linear or macrocyclic Mn<sup>2+</sup> chelates indicate that rigidity and preorganization of the ligand are key design elements to promote kinetic inertness. This made us explore bispidine (3,7-diazabicyclo[3.3.1]nonane) derivatives for Mn<sup>2+</sup> complexation. Bispidine-type chelators constitute a versatile family in coordination chemistry with a highly preorganized and rigid structure [49,50]. The bicyclic amine core can be appended with various coordinating functions and in different positions in order to match the coordination requirements of a large variety of metal ions of various sizes, coordination numbers or coordination geometries. As a function of the size and/or the position of the substituents, the bicyclic skeleton can adopt different conformations and configurations, among which the chair-chair conformer, with a “bicyclic coordination cage” is the best suited for metal complexation (Scheme 3a). Bispidines were extensively studied for the complexation of various transition metal and lanthanide ions, and many recent reports were dedicated to the development of bispidine complexes as nuclear imaging agents [51]. Interestingly, Mn<sup>2+</sup> was

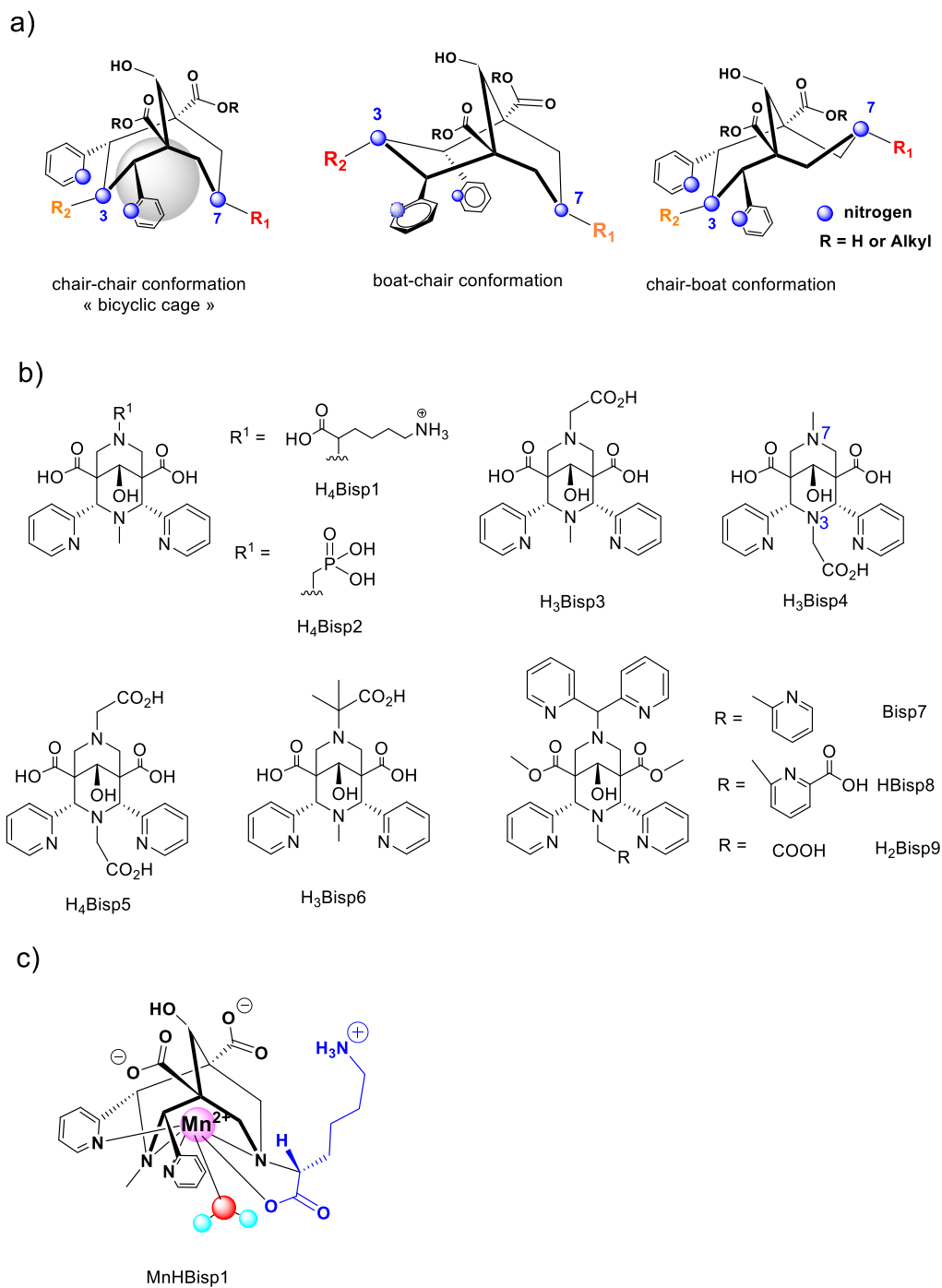
rarely in the scope of such studies, and all previous  $\text{Mn}^{2+}$ -related data were restricted to the solid state or to non-aqueous solvents.

We have first investigated the 2,4-pyridyl-disubstituted bispidol derivative  $\text{H}_4\text{Bisp1}$  bearing one carboxylate (from a lysine) for  $\text{Mn}^{2+}$  complexation [52]. This ligand can coordinate the metal in a five-dentate manner, involving the nitrogens from the two pyridines, the heterobicycle (N3 and N7) as well as the methylene carboxylate (Scheme 3), leaving one coordination site for a water molecule in the coordination sphere of the metal ion, important for good relaxivity in MRI application. The thermodynamic stability of  $\text{MnBisp1}$ , determined by pH-potentiometry, is relatively modest ( $\log K_{\text{MnL}} = 12.21$ ,  $\text{pMn} = 6.65$ ). However, once the complex is formed, it is extremely resistant to dissociation. In a standard transmetalation test carried out in the presence of 10 or 50 equiv. of  $\text{Zn}^{2+}$  at pH 6 and 37 °C, no dissociation at all was observed for 140 days, while the most inert non-bispidine chelate,  $\text{Mn}(3,9\text{-PC2A-BPEN})$  has a dissociation half-life of 64.5 h under similar conditions (37 °C, pH 6.0, 25  $\text{Zn}^{2+}$  equivalents) [47]. Such high kinetic inertness is unprecedented for a  $\text{Mn}^{2+}$  chelate.  $\text{MnHBisp1}$  (protonated on the lysine amine) has also excellent relaxation properties, comparable to those of  $\text{Gd}^{3+}$ -based agents, despite the difference in the electron spin of the metals. The two non-coordinating carboxylate groups create an additional second sphere contribution to relaxivity which, together with the slightly higher molecular weight with respect to typical small molecular weight contrast agents, is responsible for the unusually high relaxivity ( $r_1 = 4.28 \text{ mM}^{-1}\cdot\text{s}^{-1}$  and  $3.37 \text{ mM}^{-1}\cdot\text{s}^{-1}$  at 25 °C and 37 °C, respectively, 20 MHz, pH 7 in water). The *in vivo* imaging potential of  $\text{MnHBisp1}$  was evaluated in a preliminary MRI experiment in healthy mice at 7 T. Following intravenous injection of  $\text{MnHBisp1}$  at 0.06 mmol/kg dose, the signal intensity was monitored over time in various organs, which showed renal clearance and practically no liver uptake (Figure 1). This was further confirmed by *ex vivo* ICP-OES biodistribution measurements of Mn in various tissues. Moreover,  $\text{Bisp1}$  was successfully labeled with  $^{52}\text{Mn}^{2+}$ , and the radiocomplex proved to be stable in biological media. In addition to the MRI potential of  $\text{MnHBisp1}$ , this opens interesting perspectives also for immunoPET applications, after further conjugation of the

bifunctional ligand  $\text{Bisp1}$  to biomolecules, such as antibodies.

Analogous bispidine ligands bearing methylenephosphonate ( $\text{Bisp2}$ ) and methylenecarboxylate ( $\text{Bisp3}$ ) substituents instead of the lysine have been also synthesized, and their  $\text{Mn}^{2+}$  complexes have shown similarly remarkable inertness and good proton relaxivities [53].  $^{52}\text{Mn}^{2+}$  radiolabeling of the phosphonate derivative was realized with excellent yields and the radiocomplex showed high stability.

In a recent comprehensive study combining structural NMR, potentiometric, relaxometric and kinetic experiments with DFT calculations, we have addressed how the substituents on the two nitrogens of the heterobicycle (N3 and N7) affect the conformation of the  $\text{Mn}^{2+}$  complexes [54]. In these studies, we have included a series of ligands  $\text{Bisp3}$ ,  $\text{Bisp4}$  and  $\text{Bisp5}$  that possess methylenecarboxylate substituents at the N7 or N3 positions or both, respectively (Scheme 3b). We could conclude that in this family the conformation of the bispidine is determined by the nature of the N3 substituent (methyl or methylenecarboxylate), with very important consequences on the thermodynamic stability, kinetic inertness, hydration state and relaxation properties of the complexes. Only ligands without N3-appended methylenecarboxylate adopt the chair–chair conformation. Dissociation (as well as complex formation) is several orders of magnitude slower for the  $\text{Mn}^{2+}$  chelates in chair–chair conformation. The hydration number and the relaxation properties are also dependent on the ligand conformation:  $\text{Mn}^{2+}$  chelates in boat-chair conformation have less than one inner sphere water molecule, as shown by  $^{17}\text{O}$  NMR data, which is unfavorable as it results in lower relaxivities. In overall, we could evidence that chair–chair conformation is required for the favorable properties of  $\text{Mn}^{2+}$  bispidines. Another ligand,  $\text{Bisp6}$  (Scheme 3b) was also investigated to address how steric crowding introduced on the  $\alpha$  carbon of the N7 methylenecarboxylate substituent affects the kinetic inertness of the  $\text{Mn}^{2+}$  complex. As it was previously found in the family  $\text{Ln}^{3+}$ -tetraazamacrocycles [55], this modification on the methylenecarboxylate arm further increases the resistance of the  $\text{Mn}^{2+}$  chelate to dissociation, leading to a dissociation half-life which is roughly doubled for  $\text{MnBisp6}$  with respect to the  $\text{MnBisp3}$  analogue.



**Scheme 3.** (a) Bispidine conformations, (b) bispidine ligands for  $Mn^{2+}$  complexation and (c) the putative structure of  $MnHBisp1$ .

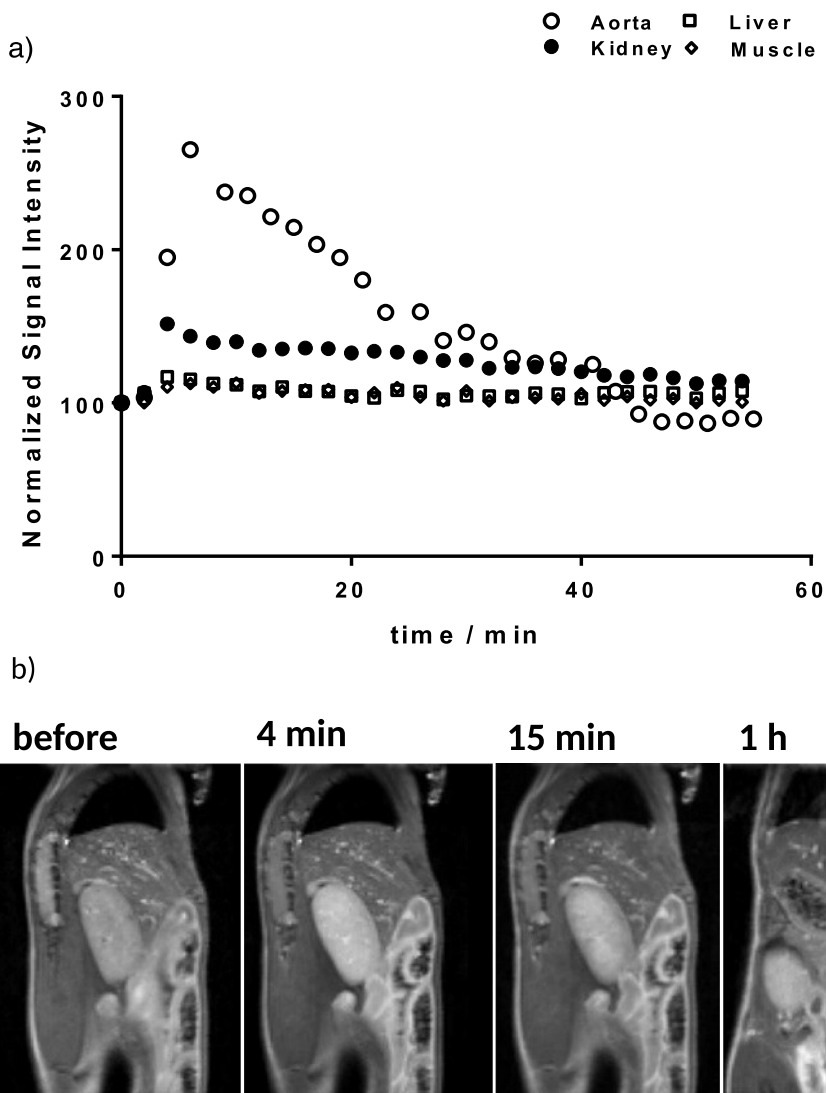


**Figure 1.** MRI of healthy mice at 7 T following intravenous injection of MnBisP1 at 0.06 mmol/kg dose. (a) Normalized signal intensity in the kidney, muscle, liver and aorta plotted as a function of time. Measurements were performed every 2 min for 4 mice. (b) Sagittal T1-weighted MR images prior to injection and at 4, 15 min and 1 h post intravenous injection of the complex. Reproduced with permission from reference [52].

Bispidine ligands of higher denticity have been also investigated for  $\text{Mn}^{2+}$  complexation and found to exhibit other extraordinary coordination chemistry features. While high kinetic inertness, as well as relatively high thermodynamic stability could be now achieved for  $\text{Mn}^{2+}$  chelates, none of them so far provided selectivity for  $\text{Mn}^{2+}$  over other transition metal ions, in particular  $\text{Zn}^{2+}$ , its major biological

competitor. This directly derives from the large ionic radius of  $\text{Mn}^{2+}$  and the spherical distribution of its  $d$  electrons. The Irving–Williams series describes the order of complex stabilities with a particular ligand in the first row of divalent transition metal cations, and  $\text{Mn}^{2+}$  complexes are usually the least stable:  $\text{Mn}^{2+} < \text{Fe}^{2+} < \text{Co}^{2+} < \text{Ni}^{2+} < \text{Cu}^{2+} > \text{Zn}^{2+}$ . We hypothesized that the rigid and preorganized nature of

bispidines make them appropriate to design ligands with high denticity and a perfectly adapted coordination cavity for the ~10% larger size of  $\text{Mn}^{2+}$  versus  $\text{Zn}^{2+}$ . This cavity would be too large for  $\text{Zn}^{2+}$ , which could not accommodate all of the donor groups in its coordination sphere. The higher number of coordinating functions would then lead to a higher stability for  $\text{Mn}^{2+}$  as compared to  $\text{Zn}^{2+}$ . Some previous observations were already in support of preferential coordination of larger metal ions by the rigid bispidine cavity, resulting in divergence from the Irving–Williams series [56,57].

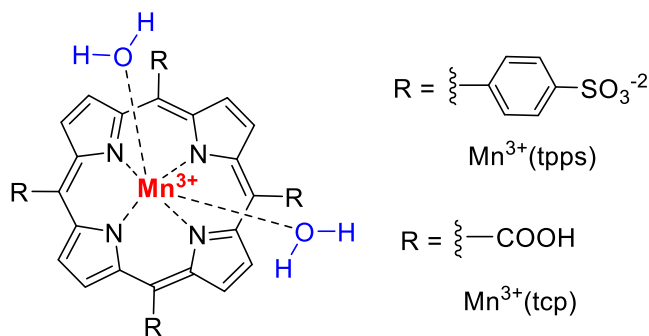
Hepta- and octadentate bispidine ligands Bisp7, Bisp8 and Bisp9 have been thus synthesized (Scheme 3) [58,59]. The  $\text{Mn}^{2+}$  and  $\text{Zn}^{2+}$  complexes have been subject of solid-state X-ray and computational studies to address their structure, and pH-potentiometric, relaxometric and kinetic investigations have been conducted to characterize their stability and inertness in aqueous solution. The solid-state structures show octadentate coordination for the  $\text{Mn}^{2+}$ , and hexadentate coordination for the  $\text{Zn}^{2+}$  complexes, evidencing that the coordination cavity provided by these ligands is well-suited for  $\text{Mn}^{2+}$  but too large for  $\text{Zn}^{2+}$ . The good match for  $\text{Mn}^{2+}$  and the misfit for  $\text{Zn}^{2+}$  was further demonstrated by empirical force field calculations which indicated that  $\text{Mn}^{2+}$  has an optimum size, while  $\text{Zn}^{2+}$  coordination induces a ligand-based strain of ~50 kJ/mol. Thermodynamic stability constants determined by pH-potentiometric ( $\text{Zn}^{2+}$ ) or relaxometric ( $\text{Mn}^{2+}$ ) titrations, further corroborated with  $^1\text{H}$  NMR and UV–Vis data, confirmed the expectations from the structural and computational studies. There is a spectacular, 5–10 orders of magnitude difference in stability in favor of the  $\text{Mn}^{2+}$  complexes over the  $\text{Zn}^{2+}$  analogues ( $\log K_{\text{MnL}} = 24.2, 24.7$  and  $19.47$  for MnBisp7, MnBisp8 and MnBisp9, versus  $\log K_{\text{ZnL}} = 14.30, 14.70$  and  $15.04$  for ZnBisp7, ZnBisp8 and ZnBisp9, respectively). These complexes represent the first examples of real  $\text{Mn}^{2+}$  selectivity in aqueous solution. The kinetic inertness of these chelates also remains excellent, though slightly lower than that of MnHBisp1.

MnBisp9 has been fully characterized for its relaxation properties [59]. Its relaxivity ( $4.44 \text{ mM}^{-1}\cdot\text{s}^{-1}$  at 20 MHz, 25 °C) is slightly superior to that of MnBisp1 which can be accounted for the 17% higher molecular weight, thus slower rotation. This overbalances

the lack of second-sphere contribution to relaxivity which operates for MnBisp1 thanks to the non-coordinating carboxylate groups, but which is not present for MnBisp9 where the carboxylates are replaced by esters. A preliminary *in vivo* MRI study has been carried out with MnBisp9 in mice at 7 T. Even at an unusually low injected dose (0.02 mmol/kg, 80% below typical doses), good contrast is observed in the kidneys. The signal variation over time indicates rapid renal clearance and no significant liver uptake. *Ex vivo* ICP-MS data point to full elimination of the complex from the mice after 24 h.

## 5. $\text{Mn}^{3+}$ complexes and redox-responsive MRI agents based on the $\text{Mn}^{2+}/\text{Mn}^{3+}$ switch

The stabilization of the  $\text{Mn}^{3+}$  state in aqueous solution and physiological pH is by far not obvious, due to the strong tendency of this cation to hydrolysis as well as to dismutation yielding  $\text{Mn}^{2+}$  and  $\text{Mn}^{4+}$ . The need for an inner sphere water in MRI applications makes stabilization even more difficult, and indeed, only few types of  $\text{Mn}^{3+}$  complexes are known with coordinated water molecule at pH 7. Among these,  $\text{Mn}^{3+}$  porphyrins represent a specific class endowed with high stability, and they were indeed considered in MRI and studied for their relaxation properties a long time ago.  $\text{Mn}^{3+}$  porphyrins have two water molecules coordinated to the metal ion, above and below the porphyrin plane. The relaxivities measured for some water soluble  $\text{Mn}^{3+}$  porphyrins such as the (5,10,15,20-tetrakis-(*p*-sulfonatophenyl) porphinate) derivative Mn(tpps) (Scheme 4) were considered as anomalously high for the given molecular size and electron spin, and this was tentatively explained by the anisotropy of the electron density at the metal center resulting in a closer approach of the  $\text{Mn}^{3+}$  spin density to the coordinated water protons [60,61]. More recently, there has been a renewed interest in  $\text{Mn}^{3+}$  porphyrins. Zhang and collaborators added carboxylates on the porphyrin periphery to increase hydrophilicity and facilitate *in vivo* clearance of the Mntcp complex (Scheme 4) [17,62]. The relaxivity, as well as the biodistribution have been modulated by further structural modifications of this carboxylated derivative, dimers endowed with HSA-binding capability have been developed for blood pool imaging [63], and specific liver targeting was generated by introducing a 4-ethoxyphenyl



**Scheme 4.** Porphyrin  $\text{Mn}^{3+}$  complexes.

substituent on the porphyrin [64]. Cell-penetrating  $\text{Mn}^{3+}$  porphyrin derivatives containing a  $\text{Zn}^{2+}$ -binding unit have been also developed and successfully used for  $\text{Zn}^{2+}$  detection [65,66]. Phtalocyanine complexes of  $\text{Mn}^{3+}$  have been also investigated [67], but like for porphyrins, water solubility remains often limited.

Mn porphyrins have been further explored in the objective of developing redox sensitive agents. The redox state is an important characteristic of tissues, and redox imbalance is associated to many pathologies which can induce oxidative stress, generate reactive oxygen species, etc. The redox homeostasis in cells and tissues is governed by different biological molecules, such as cysteine, glutathione, hydrogen peroxide, nicotinamide adenine dinucleotide (NADH), etc., and their imaging detection has great interest. Given the different relaxation properties of  $\text{Mn}^{2+}$  and  $\text{Mn}^{3+}$ , this redox pair is very promising for the design of redox sensitive MRI probes (Figure 2) [18]. For this, the system needs to satisfy several requirements, including (a) stable and inert complexation of both redox forms of the metal to prevent free metal release, (b) a redox switch of the probe which is rapid and occurs at a biologically relevant potential, and (c) a significant relaxivity change between the two redox states allowing for MRI monitoring.

Following the pioneering work by Aime and collaborators on  $\text{Mn}^{2+}/\text{Mn}^{3+}$ (tpps) [68], as well as other examples of redox responsive Mn-probes based on linear chelators such as the Janus ligand JED (Scheme 5) [69–72], we have been recently exploring a PEGylated Mn-porphyrin derivative,  $\text{Mn}(\text{pfpp}(\text{PEG})_4)$  (Scheme 5) [73]. The PEG chains

have been introduced on the molecule to increase water solubility, and additionally, fluorine atoms have been added to modulate the redox potential. Both  $\text{Mn}^{2+}$  and  $\text{Mn}^{3+}$  forms are stably complexed in aqueous solution, with a reversible switch between them. In the presence of ascorbic acid or  $\beta$ -mercaptoethanol, the  $\text{Mn}^{3+}$  form undergoes reduction, which is slowly but fully reversed in the presence of air oxygen. This is accompanied by a  $\sim 150\%$  relaxivity increase from the oxidized to the reduced form at 20 MHz. No reduction was observed with glutathione or cysteine, which can be explained by the coordination of the glutathione carboxylate to the metal ion by replacing one coordinated water molecule as evidenced by NMR data. Also,  $\text{Mn}(\text{pfpp}(\text{PEG})_4)$  had no detectable *in vitro* cytotoxicity in the typical MRI concentration range.

With such fluorinated Mn-porphyrins, the redox detection can be extended to  $^{19}\text{F}$  MRI in addition to  $^1\text{H}$  MRI, as we demonstrated with another derivative,  $\text{Mn}(\text{TPP-}p\text{-CF}_3)$  (Scheme 5) [74]. The two Mn redox states induce very different  $^1\text{H}$  and  $^{19}\text{F}$  relaxometric properties which allow for differential redox MRI detection. The  $^{19}\text{F}$  relaxation rates in these paramagnetic systems are strongly dependent on the  $\text{Mn}^{3+}\text{-F}$  distance. In  $\text{Mn}^{3+}(\text{TPP-}p\text{-CF}_3)$ , it is 9.7–10 Å, as determined from DFT calculations. This distance seems well tailored to allow for adequate paramagnetic effect of  $\text{Mn}^{3+}$  on  $^{19}\text{F}$  relaxation without excessive line-broadening, which would be detrimental for  $^{19}\text{F}$  MRI detection. Reduction of  $\text{Mn}^{3+}(\text{TPP-}p\text{-CF}_3)$  with ascorbic acid and its re-oxidation with air oxygen can be monitored by UV-Vis spectrometry,  $^{19}\text{F}$  NMR and  $^1\text{H}$  relaxivity measurements. Upon reduction, the  $^1\text{H}$  and  $^{19}\text{F}$  NMR

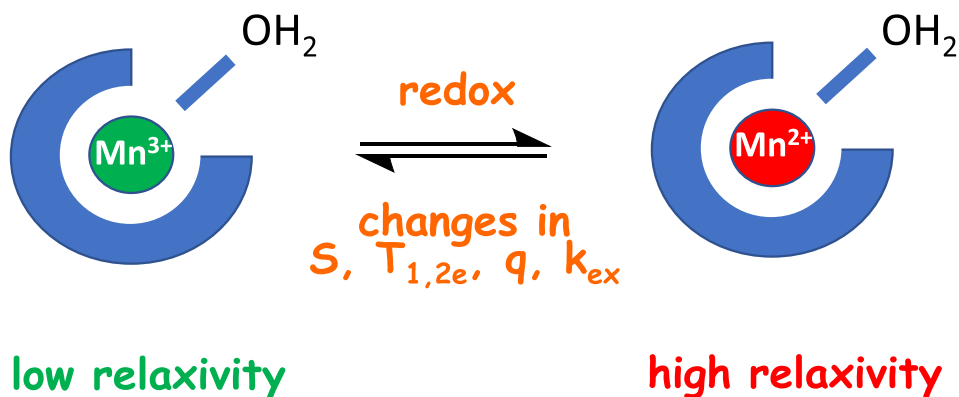
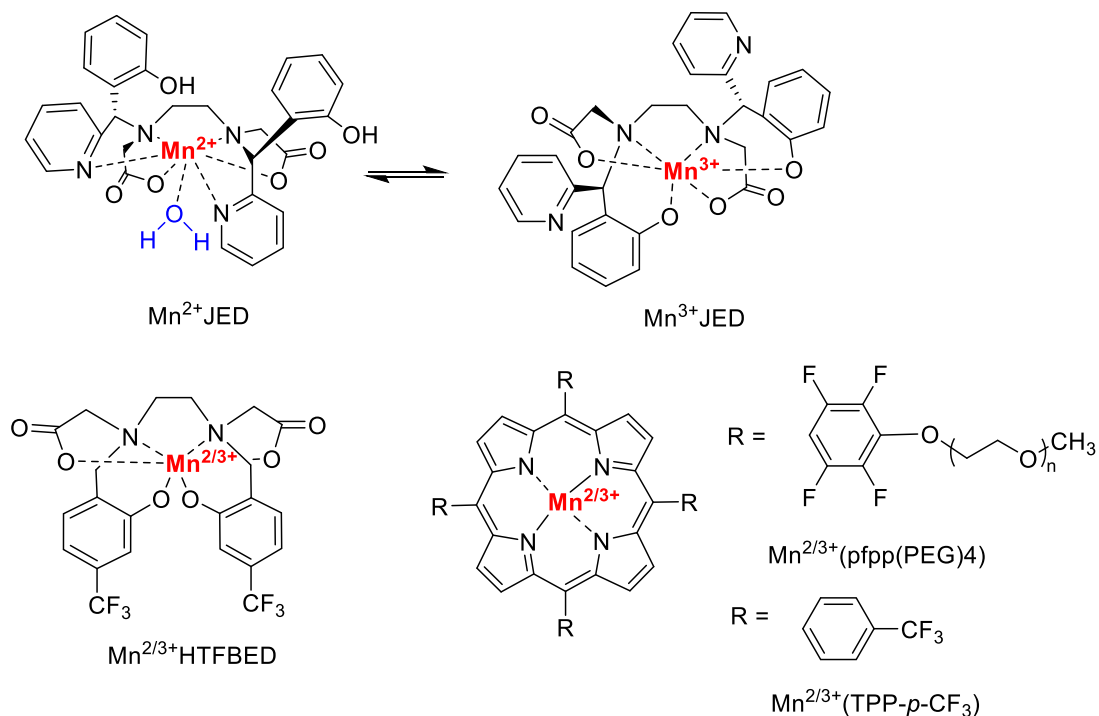


**Figure 2.** The redox switch between  $\text{Mn}^{3+}$  and  $\text{Mn}^{2+}$  states is accompanied by a change in the relaxivity of the complexes, as a consequence of variation in the electron spin ( $S$ ), electron spin relaxation times ( $T_{1,2e}$ ), hydration number ( $q$ ), or water exchange rate ( $k_{\text{ex}}$ ).



**Scheme 5.**  $\text{Mn}^{2+}/\text{Mn}^{3+}$  complexes investigated as redox responsive probes.

signals of  $\text{Mn}^{3+}(\text{TPP-}p\text{-CF}_3)$  largely broaden and disappear. The reduction/oxidation process can be readily visualized on phantom  $^{19}\text{F}$  images acquired in DMSO/water mixture (Figure 3).

$^{19}\text{F}$  MRI detection of  $\text{Mn}^{2+}/\text{Mn}^{3+}$  redox changes was also realized using the HTFBED ligand

(Scheme 5) [72]. The complexes respond to different redox active species of the biological environment including ROS, ascorbic acid or glutathione with concomitant changes in the  $^{19}\text{F}$  as well as in the  $^1\text{H}$  MRI signal intensity. In particular, an eight-fold increase of the  $^{19}\text{F}$  signal was detected upon



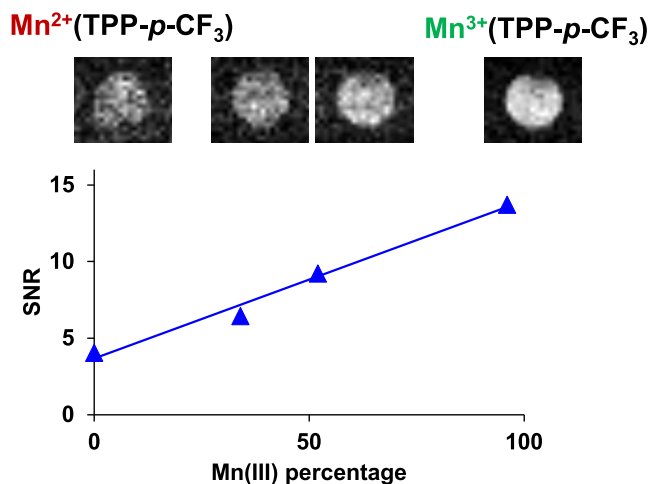


**Figure 3.** Monitoring oxidation of  $\text{Mn}^{2+}$  (TPP-*p*- $\text{CF}_3$ ) ( $c_{\text{MnL}} = 1.6$  mM in DMSO) by air oxygen. Variation of the Signal to Noise Ratio (SNR) in MRI phantoms as a function of the oxidized  $\text{Mn}^{3+}$  (TPP-*p*- $\text{CF}_3$ ) content (%). The  $^{19}\text{F}$  MRI phantom images for each point are represented above.  $B = 7$  T; TR: 60 ms; TE: 1.3 ms; FA:  $90^\circ$ ; NA: 256; acquisition time 8 min 11 s. The signal of the  $\text{Mn}^{2+}$  complex was saturated with a selective pulse. Adapted with permission from ref. [74].

oxidation from  $\text{Mn}^{2+}$  to  $\text{Mn}^{3+}$  form, and the responsive properties of these probes could be also validated at the cellular level in HepG2 cells.

## 6. Conclusion

$\text{Mn}^{2+}$  complexes represent the most viable alternatives to replace  $\text{Gd}^{3+}$ -based MRI contrast agents in the clinical practice. In this context, many chelators, including open-chain, macrocyclic and bicyclic structures, have been explored in the last years for  $\text{Mn}^{2+}$  complexation, and recently there has been important progress in substantially improving the thermodynamic stability, the selectivity and the kinetic inertness of  $\text{Mn}^{2+}$  chelates. Endowed with a highly preorganized and rigid skeleton, bispidine ligands proved to provide unprecedented properties in  $\text{Mn}^{2+}$  coordination chemistry, such as extreme kinetic inertness, complex stability and  $\text{Mn}^{2+}$  selectivity, which can be further combined with excellent relaxation properties. An increasing number of  $\text{Mn}^{2+}$  complexes are successfully characterized in *in vivo* preclinical imaging, and some of them have reached human clinical trials as potential MRI agents. The  $\text{Mn}^{3+}$  state is also increasingly explored, mainly in porphyrin complexes. Finally, efforts are still being made in order to develop Mn-based redox responsive agents.

## Declaration of interests

The authors do not work for, advise, own shares in, or receive funds from any organization that could benefit from this article, and have declared no affiliations other than their research organizations.

## References

- [1] A. Feldman, *RadioGraphics*, 1989, **9**, 1113-1128.
- [2] J. Wahsner, E. M. Gale, A. Rodríguez-Rodríguez, P. Caravan, *Chem. Rev.*, 2019, **119**, 957-1057.
- [3] E. Toth, L. Helm, A. Merbach, in *The Chemistry of Contrast Agents in Medical Magnetic Resonance Imaging* (A. Merbach, L. Helm, E. Toth, eds.), John Wiley & Sons, Chichester, 2nd ed., 2013, 25-81.
- [4] T. Grobner, *Nephrol. Dial. Transplant.*, 2006, **21**, 1104-1108.
- [5] E. Di Gregorio, G. Ferrauto, C. Furlan, S. Lanzardo, R. Nuzzi, E. Gianolio, S. Aime, *Invest. Radiol.*, 2018, **53**, 167-172.
- [6] K. Inoue, M. Fukushi, A. Furukawa, S. K. Sahoo, N. Veerasamy, K. Ichimura, S. Kasahara, M. Ichihara, M. Tsukada, M. Torii, M. Mizoguchi, Y. Taguchi, S. Nakazawa, *Marine Pollut. Bull.*, 2020, **154**, article no. 111148.
- [7] S. Le Goff, J. A. Barrat, L. Chauvaud, Y. M. Paulet, B. Gueguen, D. Ben Salem, *Sci. Rep.*, 2019, **9**, article no. 8015.
- [8] A. Gupta, P. Caravan, W. S. Price, C. Platas-Iglesias, E. M. Gale, *Inorg. Chem.*, 2020, **59**, 6648-6678.
- [9] B. Drahos, I. Lukes, E. Toth, *Eur. J. Inorg. Chem.*, 2012, 1975-1986.
- [10] P. G. Lauterbur, *Nature*, 1973, **242**, 190-191.
- [11] A. P. Korestky, A. C. Silva, *NMR Biomed.*, 2004, **17**, 527-531.

- [12] M. G. Cersosimo, W. C. Koller, *Neurotoxicology*, 2006, **27**, 340-346.
- [13] S. Lacerda, D. Ndiaye, É. Tóth, in *Advances in Inorganic Chemistry, Recent Highlights I* (C. D. Hubbard, R. Van Eldik, eds.), vol. 78, Elsevier, 2021, 109-142.
- [14] B. Drahos, J. Kotek, P. Hermann, I. Lukes, E. Toth, *Inorg. Chem.*, 2010, **49**, 3224-3238.
- [15] B. Drahos, V. Kubicek, C. S. Bonnet, P. Hermann, I. Lukes, E. Toth, *Dalton Trans.*, 2011, **40**, 1945-1951.
- [16] M. Botta, F. Carniato, D. Esteban-Gomez, C. Platas-Iglesias, L. Tei, *Future Med. Chem.*, 2019, **11**, 1461-1483.
- [17] W. Cheng, I. E. Haedicke, J. Nofiele, F. Martinez, K. Beera, T. J. Scholl, H.-L. M. Cheng, X.-a. Zhang, *J. Med. Chem.*, 2014, **57**, 516-520.
- [18] S. M. Pinto, V. Tomé, M. J. F. Calvete, M. M. C. A. Castro, É. Tóth, C. F. G. C. Geraldés, *Coord. Chem. Rev.*, 2019, **390**, 1-31.
- [19] C. M. Lewis, S. A. Graves, R. Hernandez, H. F. Valdovinos, T. E. Barnhart, W. Cai, M. E. Meyerand, R. J. Nickles, M. Suzuki, *Theranostics*, 2015, **5**, 227-239.
- [20] <https://clinicaltrials.gov/ct2/show/NCT05413668>.
- [21] <https://www.gehealthcare.com/about/newsroom/press-releases/ge-healthcare-announces-completion-of-phase-i-subject-recruitment-in-early-clinical-development-program-for-a-first-of-its-kind-macrocyclic-manganese-based-mri-contrast-agent>.
- [22] M. S. Zetter, E. J. Wood, J. P. Hunt, H. W. Dodgen, M. W. Grant, *Inorg. Chem.*, 1972, **11**, 2701-2706.
- [23] M. K. Islam, S. Kim, H. K. Kim, Y. H. Kim, Y. M. Lee, G. Choi, A. R. Baek, B. K. Sung, M. Kim, A. E. Cho, H. Kang, G. H. Lee, S. H. Choi, T. Lee, J. A. Park, Y. Chang, *Bioconj. Chem.*, 2018, **29**, 3614-3625.
- [24] M. K. Islam, S. Kim, H.-K. Kim, S. Park, G.-H. Lee, H. J. Kang, J.-C. Jung, J.-S. Park, T.-J. Kim, Y. Chan, *J. Med. Chem.*, 2017, **60**, 2993-3001.
- [25] S. Aime, P. L. Anelli, M. Botta, M. Brocchetta, S. Canton, F. Fedeli, E. Gianolio, E. Terreno, *J. Biol. Inorg. Chem.*, 2002, **7**, 58-67.
- [26] F. K. Kalman, G. Tircso, *Inorg. Chem.*, 2012, **51**, 10065-10067.
- [27] J. Charlier, E. Merciny, J. Fuger, *Anal. Chim. Acta*, 1985, **178**, 299-306.
- [28] E. Molnar, B. Varadi, Z. Garda, R. Botar, F. K. Kalman, E. Toth, C. Platas-Iglesias, I. Toth, E. Brucher, G. Tircso, *Inorg. Chim. Acta*, 2018, **472**, 254-263.
- [29] C. Vanasschen, E. Molnar, G. Tircso, F. K. Kalman, E. Toth, M. Brandt, H. H. Coenen, B. Neumaier, *Inorg. Chem.*, 2017, **56**, 7746-7760.
- [30] K. Pota, Z. Garda, F. K. Kalman, J. L. Barriada, D. Esteban-Gomez, C. Platas-Iglesias, I. Toth, E. Brucher, G. Tircso, *New J. Chem.*, 2018, **42**, 8001-8011.
- [31] S. Laine, C. S. Bonnet, F. K. Kalman, Z. Garda, A. Pallier, E. Caille, F. Suzenet, G. Tircso, E. Toth, *New J. Chem.*, 2018, **42**, 8012-8020.
- [32] S. W. McRae, M. Cleary, D. DeRoche, F. M. Martinez, Y. Xia, P. Caravan, E. M. Gale, J. A. Ronald, T. J. Scholl, *J. Med. Chem.*, 2023, **66**, 6567-6576.
- [33] E. M. Gale, I. P. Atanasova, F. Blasi, I. Ay, P. Caravan, *J. Am. Chem. Soc.*, 2015, **137**, 15548-15557.
- [34] E. M. Gale, H.-Y. Wey, I. Ramsay, Y.-F. Yen, D. E. Sosnovik, P. Caravan, *Radiology*, 2018, **286**, 877-884.
- [35] D. J. Erstad, I. A. Ramsay, V. C. Jordan, M. Sojoodi, B. C. Fuchs, K. K. Tanabe, P. Caravan, E. M. Gale, *Invest. Radiol.*, 2019, **54**, 697-703.
- [36] B. P. Bonner, S. R. Yurista, J. Coll-Font, S. Chen, R. A. Eder, A. N. Foster, K. D. Nguyen, P. Caravan, E. M. Gale, C. Nguyen, *J. Am. Heart Assoc.*, 2023, **12**, article no. e026923.
- [37] J. Wang, H. Wang, I. A. Ramsay, D. J. Erstad, B. C. Fuchs, K. K. Tanabe, P. Caravan, E. M. Gale, *J. Med. Chem.*, 2018, **61**, 8811-8824.
- [38] S. Chirayil, V. C. Jordan, A. F. Martins, N. Paranawithana, S. J. Ratnakar, A. D. Sherry, *Inorg. Chem.*, 2021, **60**, 2168-2177.
- [39] S. Anbu, S. H. L. Hoffmann, F. Carniato, L. Kenning, T. W. Price, T. J. Prior, M. Botta, A. F. Martins, G. J. Stasiuk, *Angew. Chem. Int. Ed.*, 2021, **60**, 10736-10744.
- [40] A. Bianchi, L. Calabi, C. Giorgi, P. Losi, P. Mariani, D. Palano, P. Paoli, P. Rossi, B. Valtancoli, *J. Chem. Soc. Dalton Trans.*, 2001, 917-922.
- [41] G. A. Rolla, C. Platas-Iglesias, M. Botta, L. Tei, L. Helm, *Inorg. Chem.*, 2013, **52**, 3268-3279.
- [42] Z. Garda, A. Forgacs, Q. N. Do, F. K. Kalman, S. Timari, Z. Baranyai, L. Tei, I. Toth, Z. Kovacs, G. Tircso, *J. Inorg. Biochem.*, 2016, **163**, 206-213.
- [43] G. Rolla, V. De Biasio, G. B. Giovenzana, M. Botta, L. Tei, *Dalton Trans.*, 2018, **47**, 10660-10670.
- [44] B. Drahos, J. Kotek, I. Cisarova, P. Hermann, L. Helm, I. Lukes, E. Toth, *Inorg. Chem.*, 2011, **50**, 12785-12801.
- [45] Z. Garda, E. Molnár, N. Hamon, J. L. Barriada, D. Esteban-Gómez, B. Váradi, V. Nagy, K. Pota, F. K. Kálmán, I. Tóth, N. Lih, C. Platas-Iglesias, É. Tóth, R. Tripiér, G. Tircsó, *Inorg. Chem.*, 2021, **60**, 1133-1148.
- [46] R. Botár, E. Molnár, G. Trencsényi, J. Kiss, F. K. Kálmán, G. Tircsó, *J. Am. Chem. Soc.*, 2020, **142**, 1662-1666.
- [47] R. Botár, E. Molnár, Z. Garda, E. Madarasi, G. Trencsényi, J. Kiss, F. K. Kálmán, G. Tircsó, *Inorg. Chem. Front.*, 2022, **9**, 577-583.
- [48] F. K. Kálmán, V. Nagy, B. Váradi, Z. Garda, E. Molnár, G. Trencsényi, J. Kiss, S. Mème, V. Mème, É. Tóth, G. Tircsó, *J. Med. Chem.*, 2020, **63**, 6057-6065.
- [49] P. Comba, M. Kerscher, W. Schiek, in *Progress in Inorganic Chemistry* (K. D. Karlin, ed.), vol. 55, John Wiley & Sons, 2007, 613-704.
- [50] A. M. Nonat, A. Roux, M. Sy, L. J. Charbonniere, *Dalton Trans.*, 2019, **48**, 16476-16492.
- [51] P. Comba, M. Kerscher, K. Rueck, M. Starke, *Dalton Trans.*, 2018, **47**, 9202-9220.
- [52] D. Ndiaye, M. Sy, A. Pallier, S. Meme, I. de Silva, S. Lacerda, A. M. Nonat, L. J. Charbonniere, E. Toth, *Angew. Chem. Int. Ed.*, 2020, **59**, 11958-11963.
- [53] M. Sy, D. Ndiaye, I. da Silva, S. Lacerda, L. J. Charbonniere, É. Tóth, A. M. Nonat, *Inorg. Chem.*, 2022, **61**, 13421-13432.
- [54] D. Ndiaye, M. Sy, W. Thor, L. J. Charbonniere, A. M. Nonat, E. Toth, *Chem. Eur. J.*, 2023, **29**, article no. e202301880.
- [55] S. Aime, M. Botta, Z. Garda, B. E. Kucera, G. Tircso, V. G. Young, M. Woods, *Inorg. Chem.*, 2011, **50**, 7955-7965.
- [56] P. Comba, H. Rudolf, H. Wadepohl, *Dalton Trans.*, 2015, **44**, 2724-2736.

- [57] P. Comba, M. Kerscher, K. Rück, M. Starke, *Dalton Trans.*, 2018, **47**, 9202-9220.
- [58] P. Cieslik, P. Comba, B. Dittmar, D. Ndiaye, É. Tóth, G. Velmugan, H. Wadepohl, *Angew. Chem. Int. Ed.*, 2022, **61**, article no. e202115580.
- [59] D. Ndiaye, P. Cieslik, H. Wadepohl, A. Pallier, S. Mème, P. Comba, É. Tóth, *J. Am. Chem. Soc.*, 2022, **144**, 22212-22220.
- [60] S. H. Koenig, C. Baglin, R. D. Brown, *Magn. Reson. Med.*, 1984, **1**, 496-501.
- [61] S. H. Koenig, R. D. Brown Iii, M. Spiller, *Magn. Reson. Med.*, 1987, **4**, 252-260.
- [62] W. Cheng, T. Ganesh, F. Martinez-Santesteban, J. Lam, H. Yoon, R. Macgregor, T. Scholl, H.-L. Cheng, X.-A. Zhang, *J. Biol. Inorg. Chem.*, 2014, **19**, 229-235.
- [63] H. L. Liu, W. R. Cheng, S. L. Dong, D. F. Xu, K. Tang, X. A. Zhang, *Pharmaceuticals*, 2020, **13**, 282-293.
- [64] N. N. Nystrom, H. L. Liu, F. M. Martinez, X. A. Zhang, T. J. Scholl, J. A. Ronald, *J. Med. Chem.*, 2022, **65**, 9846-9857.
- [65] T. Lee, X.-a. Zhang, S. Dhar, H. Faas, S. J. Lippard, A. Jasanoff, *Chem. Biol.*, 2010, **17**, 665-673.
- [66] X.-a. Zhang, K. S. Lovejoy, A. Jasanoff, S. J. Lippard, *Proc. Natl. Acad. Sci. USA*, 2007, **104**, 10780-10785.
- [67] S. M. A. Pinto, V. A. Tomé, M. J. F. Calvete, M. M. Pereira, H. D. Burrows, A. M. S. Cardoso, A. Pallier, M. M. C. A. Castro, É. Tóth, C. F. G. C. Geraldes, *J. Inorg. Biochem.*, 2016, **154**, 50-59.
- [68] S. Aime, M. Botta, E. Gianolio, E. Terreno, *Angew. Chem. Int. Ed.*, 2000, **39**, 747-750.
- [69] E. M. Gale, C. M. Jones, I. Ramsay, C. T. Farrar, P. Caravan, *J. Am. Chem. Soc.*, 2016, **138**, 15861-15864.
- [70] E. M. Gale, S. Mukherjee, C. Liu, G. S. Loving, P. Caravan, *Inorg. Chem.*, 2014, **53**, 10748-10761.
- [71] G. S. Loving, S. Mukherjee, P. Caravan, *J. Am. Chem. Soc.*, 2013, **135**, 4620-4623.
- [72] H. Chen, X. Tang, X. Gong, D. Chen, A. Li, C. Sun, H. Lin, J. Gao, *Chem. Commun.*, 2020, **56**, 4106-4109.
- [73] S. M. A. Pinto, M. J. F. Calvete, M. E. Ghica, S. Soler, I. Gallardo, A. Pallier, M. B. Laranjo, A. M. S. Cardoso, M. M. C. A. Castro, C. M. A. Brett, M. M. Pereira, É. Tóth, C. F. G. C. Geraldes, *Dalton Trans.*, 2019, **48**, 3249-3262.
- [74] S. M. A. Pinto, A. R. R. Ferreira, D. S. S. Teixeira, S. C. C. Nunes, A. de Carvalho, J. M. S. Almeida, Z. Garda, A. Pallier, A. Pais, C. M. A. Brett, E. Tóth, M. P. M. Marques, M. M. Pereira, C. Geraldes, *Chem. Eur. J.*, 2023, **29**, article no. e202301442.